

Title	Microseismic Activity and Spatial Distribution of Coda-Q in the Westernmost Part of the North Anatolian Fault Zone, Turkey
Author(s)	NISHIGAMI, Kin'ya; ITO, Yoshihisaho; GURBUZ, Cemil; PINAR, Ali; AYBEY, Naz; UCER, S. Balamir; HONKURA, Yoshimori; ISIKARA, A. Mete
Citation	Bulletin of the Disaster Prevention Research Institute (1990), 40(2): 41-56
Issue Date	1990-06
URL	<a href="http://hdl.handle.net/2433/124968">http://hdl.handle.net/2433/124968</a>
Right	
Type	Departmental Bulletin Paper
Textversion	publisher

## Microseismic Activity and Spatial Distribution of Coda- $Q$ in the Westernmost Part of the North Anatolian Fault Zone, Turkey

By Kin'ya NISHIGAMI, Yoshihisa IIO, Cemil GÜRBÜZ, Ali PINAR, Naz AYBEY,  
S. Balamir ÜÇER, Yoshimori HONKURA and A. Mete IŞIKARA

(Manuscript received on May 23, 1990)

### Abstract

We carried out a short-term observation of microearthquakes in the seismic gap region in the westernmost part of the North Anatolian fault zone. In this region, the North Anatolian fault zone branches into two fault zones: the Izmit-Sapanca fault zone on the north, and the Iznik-Mekece fault on the south. The results of our analyses are as follows: (1) Microseismic activity was much higher along the Izmit-Sapanca fault zone than along the Iznik-Mekece fault. (2) A fault plane solution of strike-slip type was obtained for a microearthquake along the Iznik-Mekece fault. On the other hand, the solutions of both strike-slip and normal-faulting types were determined for microearthquakes along the Izmit-Sapanca fault zone. (3) Relatively lower coda- $Q$  values were estimated around the Izmit-Sapanca and Iznik-Mekece fault zones, compared with the values in the region north of the fault zones. This attenuation property is considered to be closely related to the inhomogeneity of the crust, probably due to the earthquake faulting along the North Anatolian fault zone.

Seen from the above result (2), we may estimate the faulting type of the future large earthquake in the seismic gap region as follows: If it occurs along the Iznik-Mekece fault, it will have a strike-slip mechanism; but if it occurs along the Izmit-Sapanca fault zone, its faulting type may have two possibilities, strike-slip or normal-slip.

### 1. Introduction

The North Anatolian fault is a right-lateral transform fault between the Anatolian and Eurasian plates, extending for more than 1,200 km across northern Turkey (**Fig. 1**). Since the 1939 Ercincan earthquake ( $M7.9$ ), successive large earthquakes migrated in both west and east directions, and have fractured most segments of the fault<sup>4,20</sup>. According to Toksöz *et al.*<sup>20</sup>, two segments remain unbroken (around 29°–30.5°E, and 42°–43°E) and these areas are considered to be the seismic gaps of the first kind.

The western part of the North Anatolian fault zone corresponds to one of the seismic gaps, as shown in **Fig. 1(a)**. **Fig. 1(b)** shows the detailed map around the seismic gap region. The 1967 Mudurnu earthquake ( $M7.1$ ) was the last of the westward migrating sequence of large earthquakes along the fault zone. The North Anatolian fault zone branches off into two faults westward around the end of the 1967 Mudurnu earthquake. The northern branch, which is called the Izmit-Sapanca fault zone, is situated in Quaternary basins through Izmit Bay and Sapanca Lake, and has a deformation zone as wide as 5–8 km<sup>10</sup>. The southern branch, which is called the Iznik-Mekece fault, seems to be a simple right-lateral strike-slip fault with

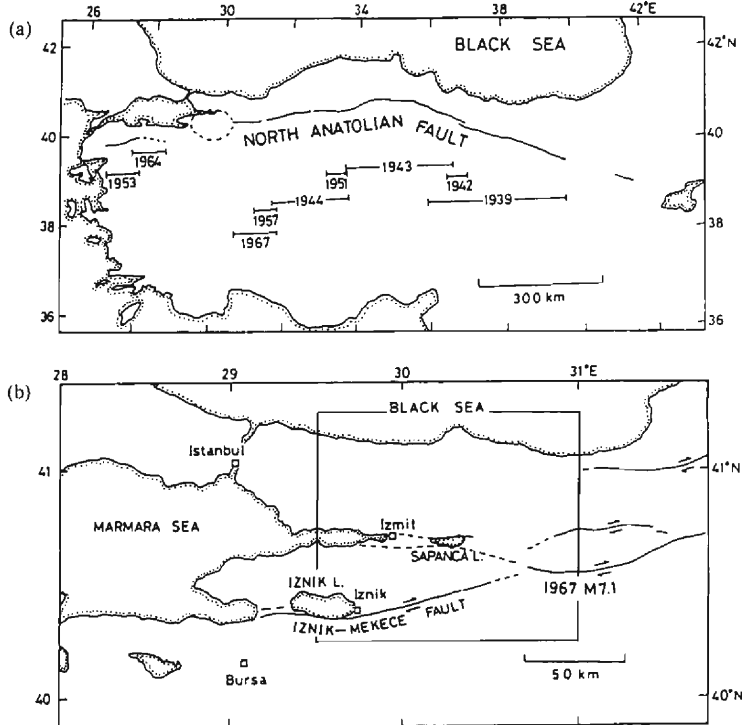


Fig. 1. Map showing the location of the North Anatolian fault zone and the area studied (after Tsukuda *et al.*<sup>22</sup>). (a) Westward migration of large earthquakes along the North Anatolian fault zone, after the 1939 Ercincan earthquake<sup>4</sup>. The area enclosed by the broken line is the seismic gap proposed by Toksöz *et al.*<sup>20</sup>. (b) Map of the area around the seismic gap region shown in (a). Solid lines denote fault traces of strike-slip type with the slip direction; broken lines show those with low clarity<sup>10</sup>. The area studied in this paper is represented by a square.

a cumulative strike separation of about 25 km<sup>19</sup>).

It is supposed that the next large earthquake may occur in the seismic gap region shown in **Fig. 1**. Several kinds of research such as geomorphological, geomagnetic and microseismic ones, and so on, have been done in this region in order to obtain basic information on future large earthquakes<sup>7,8,22</sup>. According to Crampin *et al.*<sup>5</sup> and Tsukuda *et al.*<sup>22</sup>, micro seismicity is rather high along the Izmit-Sapanca fault zone, especially near Izmit Bay; on the other hand, the Iznik-Mekece fault is quite aseismic. The latter may be interpreted as precursory seismic quiescence.

However, the tectonic situation in this region is not simple. All the large earthquakes shown in **Fig. 1(a)** had right-lateral strike-slip fault plane solutions, except for the event of 1964, which had a pure normal-faulting solution with T-axes in almost NE-SW direction<sup>12,15,16</sup>. Fault plane solutions of microearthquakes suggest similar regional characteristics<sup>6,25</sup>. The geomorphological observations show

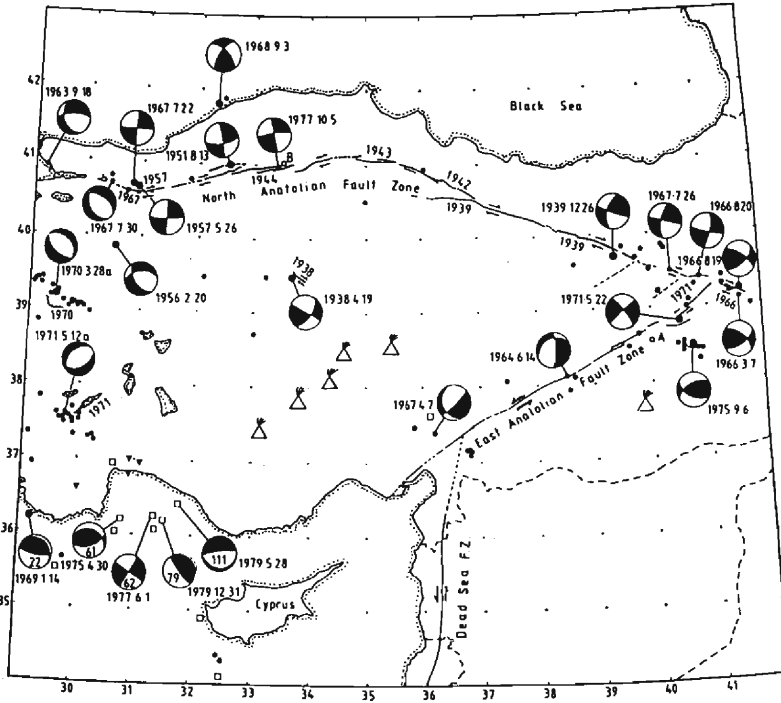


Fig. 2. Fault plane solutions (equal area projection on the lower hemisphere) of some large earthquakes in Turkey (after Jackson and McKenzie<sup>12</sup>). The events of July 22 and July 30, 1967 are the Mudurnu earthquake ( $M7.1$ ) and its largest aftershock ( $M5.6$ ), respectively. Solid circles show epicenters during the period from 1961 to 1980 (larger symbols with  $M$  6.0 or greater, smaller ones with  $M$  5.0 or greater). Open squares show those with focal depths deeper than 50 km (numbers in the dilatational quadrants of the mechanisms are the focal depths). Smoking triangles represent Quaternary volcanoes. Faults known to be active are marked with continuous lines, with dates next to them where they were activated during specific earthquakes.

that Quaternary basins and active faults of the normal-slip type extend in the east-west direction near the Marmara Sea region<sup>10</sup>). Thus, the westernmost part of Turkey, westward around 30°E, is considered to be under tensile tectonic stress in an almost north-south direction, as shown in **Fig. 2**. The seismic gap region shown in **Fig. 1** is situated in the transition zone of this tectonic stress field. It is important to elucidate the detailed tectonics in this region, in order to estimate the faulting type of the future large earthquake occurring there.

We carried out a short-term observation of microearthquakes around the western extension of the 1967 Mudurnu earthquake fault, in the summer of 1988. Our purpose is to investigate the seismic properties and the detailed tectonics in the seismic gap region. In this study, we examine the microseismicity, fault plane solutions, and attenuation property of seismic waves deduced from coda waves.

## 2. Microseismic Activity

### 2.1 Observation

We set up nine temporary microseismic stations around the western extension of the 1967 Mudurnu earthquake fault, as shown in **Fig. 3**. Details of the observation system are described in Iio *et al.*<sup>9)</sup>.

The seismometers were moving-coil velocity transducers with a natural frequency of 2 Hz. Waveform signals at station Nos. 1–5 were transmitted to the station No. 6 by radio telemeters of FM-type, and were recorded on magnetic tapes through a delay unit with a sampling frequency of 256 Hz. At stations with Nos. 7–9, seismic signals were recorded by individual event-recorder systems (OM-2) developed by Oike and Matsumura<sup>17)</sup>. The overall frequency characteristics for the both observation systems are flat between about 2 and 30 Hz. Three-component seismic waves were observed at the station No. 6, with some low gain records, and only the vertical component was observed at the other eight stations.

Our short-term network was operated from July 16 to September 30, 1988.

### 2.2 Hypocentral Distribution

**Fig. 4** shows the epicentral distribution of microearthquakes during the obser-

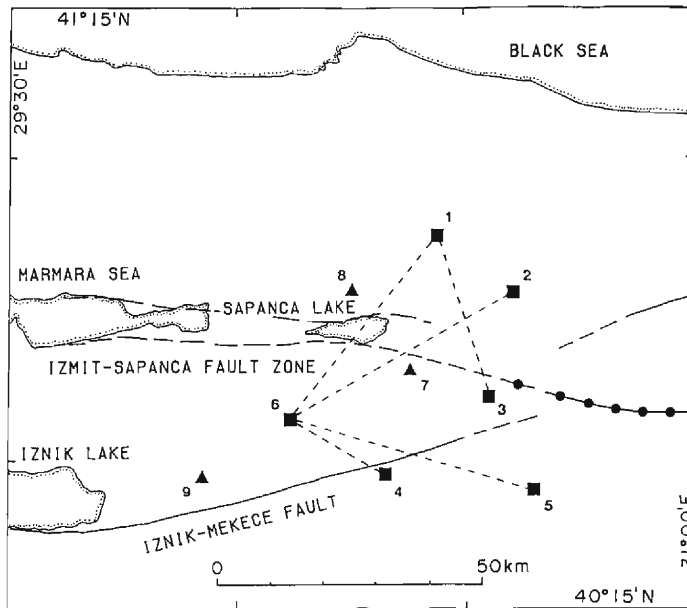


**Fig. 3.** Map showing the area studied (squared area in **Fig. 1(b)**) and temporary microseismic stations. Solid squares (1–6) represent the stations radio-linked to the station No. 6; solid triangles (7–9), independent stations. Active faults are shown by solid and broken lines. The solid line with small solid circles denotes the surface rupture associated with the 1967 Mudurnu earthquake<sup>10)</sup>.

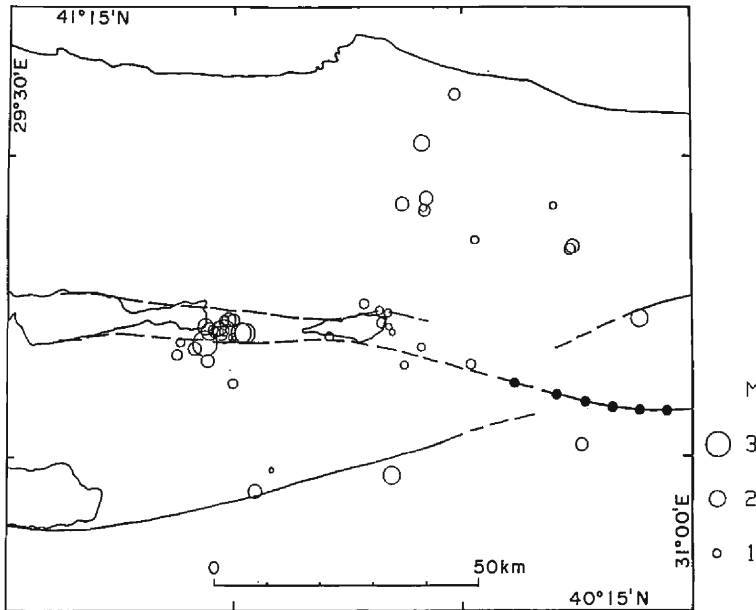


Fig. 4. Epicentral distribution of 47 microearthquakes during the period from July 16 to September 30, 1988 (after Iio *et al.*<sup>9)</sup>).

vation period, determined by Iio *et al.*<sup>9)</sup>. In this calculation, P- and S-arrival times only at six radio-linked stations were used, and a half space with the P-wave velocity of 6.0 km/s and the Poisson's ratio of 0.25 were assumed, since the velocity structure is poorly known in this region<sup>23)</sup>. Almost all the focal depths were calculated to be between about 5 and 15 km. Magnitudes were estimated from the maximum velocity amplitudes, using the formula given by Watanabe<sup>24)</sup>.

Microearthquakes seem to be distributed along the active faults as shown in

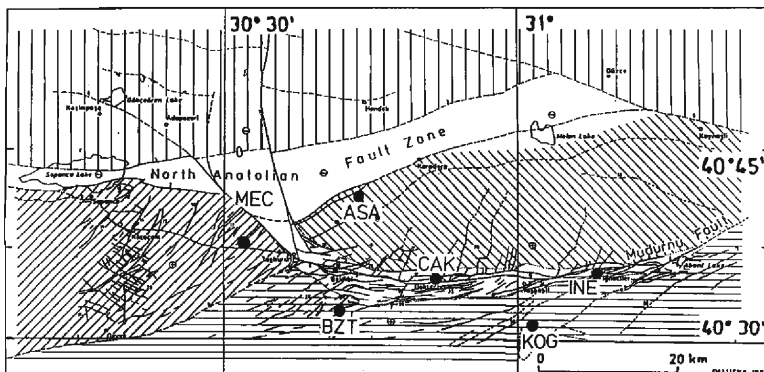
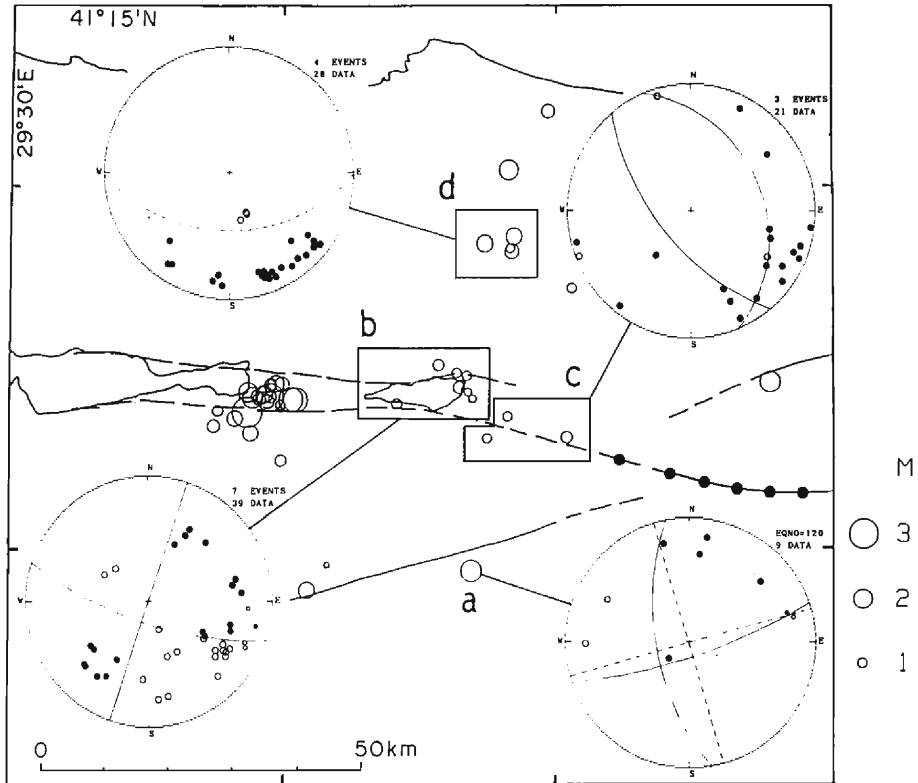


Fig. 5. Map showing the location of German microseismic stations (modified after Weigelt *et al.*<sup>25)</sup>). Data of six stations denoted by solid circles were also used in determining the focal mechanism in this study. Shaded areas represent different geological blocks.

**Fig. 4.** Seismicity is much higher along the Izmit-Sapanca fault zone, especially near Izmit Bay and Sapanca Lake, than along the Iznik-Mekece fault. This feature seems to have continued over the past several years in the view of previous research<sup>22,23</sup>.

### 2.3 Fault plane solution

The focal mechanism of microearthquakes was determined using the data of our nine stations shown in **Fig. 3**, and of six German stations operating in the Murdurnu Valley (**Fig. 5**). The velocity structure was assumed to be a homogeneous half space, because of the lack of information about it. The focal mechanism for an event ( $M_{2.2}$ ) near the Iznik-Mekece fault is shown in **Fig. 6** (event (a)). In spite of scarce data, the fault plane solution of strike-slip type is suggested. This



**Fig. 6.** Fault plane solution and composite ones, projected onto the upper hemisphere of the Wulff net, for an event or events in three regions indicated in the seismicity map (same as in **Fig. 4**). Solid and open circles represent compressional and dilatational P-wave first motions, respectively. Small symbols denote ambiguous onsets. (a) Solution for an event on Aug. 27 (07h 39 m, local time) near the Iznik-Mekece fault. Two sets of possible nodal lines are drawn. (b) Composite solution for seven events near Sapanca Lake. (c) Composite solution for three events east of Sapanca Lake. (d) Composite solution for four events north of the Izmit-Sapanca fault zone. Only one of the possible nodal lines is drawn.

solution agrees well with the geomorphological observations of the right-lateral strike-slip faulting along the Iznik-Mekece fault.

The composite focal mechanism for seven events near Sapanca Lake is shown in **Fig. 6** (region (b)). This solution is also nearly a strike-slip type. On the other hand, the three events east of Sapanca Lake, inside region (c) in **Fig. 6**, show inconsistent polarity data with this solution. The composite solution for the three events indicates a normal-faulting type, although the solution has some uncertainty.

The composite focal mechanism for four events on the north of the fault zone is shown in **Fig. 6** (region (d)). This suggests a normal-faulting solution with T-axes in an almost north-south direction, although the data distribution is quite insufficient to verify this.

### 3. Coda-Q Estimates

#### 3.1 Method

Coda waves immediately following the direct P- or S-waves are interpreted as scattered waves from inhomogeneity in the crust and the upper mantle. In this study, we analyzed coda waves after direct S-waves. Under the assumption of a single back-scattering process and of a conversion only from S- to S-waves, the coda amplitude  $u(f, t)$  for a specific frequency  $f$  is approximately expressed as follows:

$$u(f, t) = c \cdot t^{-b} \cdot \exp(-\pi \cdot f \cdot t / Q), \quad (1)$$

where  $c$  is a constant concerning the strength of radiation from the seismic source and also the intensity of scattering,  $t$  is the lapse time measured from the earthquake origin time, and  $Q$  is the quality factor of attenuation, called coda- $Q^{1,3}$ . The parameter  $b$  is related to the geometrical spreading factor of seismic waves and should be 1.0 for body waves and 0.5 for surface waves. Equation (1) is converted into the following logarithmic form:

$$\ln u(f, t) + b \cdot \ln t = \ln c - \pi \cdot f \cdot t / Q. \quad (2)$$

The  $Q$  value is obtained from a slope of this linear relationship between the coda amplitude modified above and the lapse time  $t$ .

The events used for the present analysis are shown in **Table 1**. Seismic waves were digitized at a sampling frequency of every 100 Hz, taking account of the frequency response of the observation system.

An example of processed waveforms is shown in **Fig. 7**. The coda part was taken out for analysis and resolved into nine frequency components by using a Chebyshev-type band-pass filter, as shown in **Fig. 7(a)**. The filter was applied both forward and backward along the time axis, to obtain a result with no phase delay. The decay rate of the band-pass filter was taken to be rather sharp,  $-180$  dB/oct. The smoothed coda amplitude  $u(f, t)$  in the equation (1) was obtained from filtered seismograms by running root-mean-square processing, in the same way as in Tsuku-



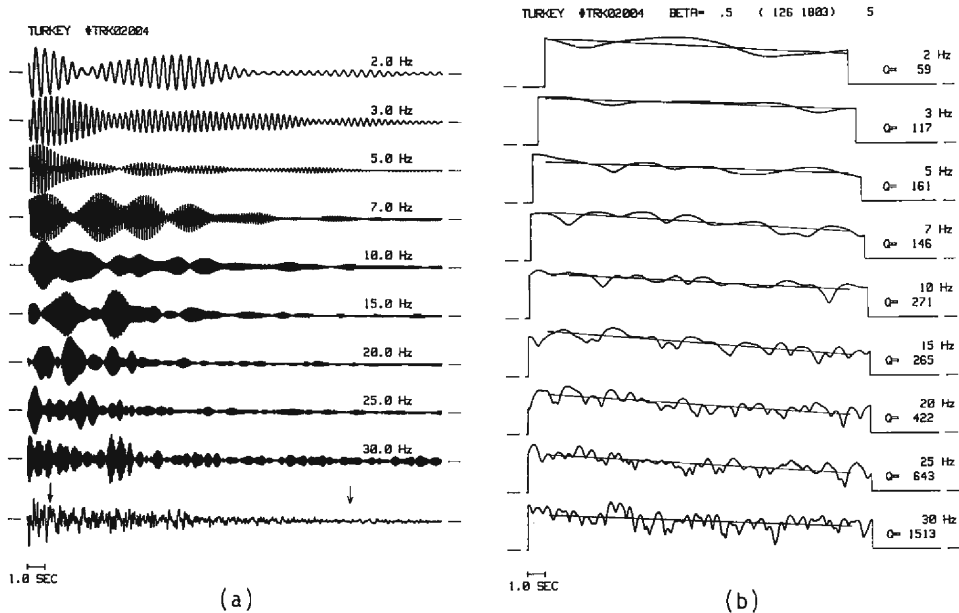


Fig. 7. (a) An example of original (bottom) and band-pass filtered coda waveforms, which correspond to data No. 9 in **Table 1**. Center frequencies of filtered ones are from 2 to 30 Hz. Amplitudes are normalized for each trace. The analysis interval for coda- $Q$  estimation is indicated by arrows on the bottom trace. (b) Logarithmic coda amplitude after the geometrical spreading effect ( $b=0.5$ ) is corrected from the filtered seismograms shown in (a). The straight line is fitted to the decay curve for each frequency component in the sense of least squares. Amplitudes are normalized for each trace and the time axis is common with that in (a).

da *et al.*<sup>22)</sup>. The length of the moving time window was taken as five times the center period of the waves. **Fig. 7(b)** represents the logarithmic amplitude in which the geometrical spreading effect is corrected by the left side of the equation (2). In this calculation, we tested the two cases of  $b=0.5$  and 1.0 for all the events analyzed. When  $b$  was taken to be 1.0, the obtained coda- $Q$  showed systematically larger values by about 20–50%, and the result on spatial distribution of coda- $Q$  differs little from that for  $b=0.5$ . In this paper, therefore, we show the result for  $b=0.5$ . Each line segment in **Fig. 7(b)** shows the linear decay of amplitude, calculated in the sense of least squares.

Equation (1) approximately holds when the lapse time is greater than about twice the travel time of direct S-waves, because of nonspherical radiation from seismic sources<sup>3)</sup>. For this reason, the initial time of the analysis interval, i.e., the left-hand arrow shown in **Fig. 7(a)**, was taken to be about 1.5–2.0 times as large as the direct S-wave arrivals measured from the event origin time. We took rather short analysis intervals, 15–20 sec, to increase the spatial resolution of coda- $Q$ .

### 3.2 Results

Table 1. List of event-station pairs in coda- $Q$  analysis in this study. Numbers at the left correspond to those in **Fig. 8**. Origin times of events are the local time. Station numbers are those in **Fig. 3**.  $Q$  values obtained at 5 and 10 Hz, and corresponding subregion name are also shown.

No.	Event				Station No.	Coda- $Q$		Subregion
	Origin time	Depth (km)	$M$			5 Hz	10 Hz	
1	Jul. 16	21:18	17.5	1.5	5	97	180	B
2	Jul. 28	04:22	22.9	1.7	1	122	453	A
3	Aug. 6	10:43	7.9	1.2	7	120	245	B
4	Aug. 11	23:36	7.2	1.7	8	290	528	A
5	Aug. 17	23:32	4.3	1.0	7	83	176	B
6	Aug. 20	20:44	5.5	>2.2	7	210	231	B
7					9	115	297	B
8	Aug. 27	07:39	6.7	2.2	3	207	296	B
9					4	161	271	B
10					6	122	238	B
11	Aug. 27	20:27	6.0	1.3	6	140	238	B
12	Sep. 4	19:09	6.4	1.4	1	260	378	A

We obtained frequency-dependent  $Q$  values for twelve event-station pairs shown in **Table 1** and **Fig. 8**.  $Q$  values obtained at 5 and 10 Hz are listed in **Table 1**. When coda waves are interpreted as single back-scattered waves, the  $Q$  values obtained reflect the average attenuation property inside an elliptic (surface waves) or ellipsoidal (body waves) area. In the case of large lapse time from an event origin time, this area has almost a circular or spherical shape, centered at the midpoint between a hypocenter and a station. The radius  $r$  is approximately expressed by the lapse time  $t$  and the average velocity  $v$  of surface waves or S-waves as follows:

$$r = v \cdot t / 2 . \tag{3}$$

In our present study, this area corresponds to a doughnut-shaped “coda-generating area” near the surface and  $v$  was taken to be 3.5 km/s. The maximum radius, which is determined by the final time of the analysis interval, is estimated to be 30–55 km. The width of the area is also estimated, and is 20–35 km in a horizontal direction. Such wide areas for the respective event-station pairs analyzed overlap each other to a great extent.

**Fig. 8** shows the spatial distribution of  $Q$  values obtained at 10 Hz. This region may be divided into two subregions A and B, from a standpoint of the attenuation property of seismic waves. The extent of each subregion is represented by a composite circular arc, which is obtained by superposing the “coda-generating areas” of all the event-station pairs concerned. In calculating the radius from equation (3), we used the median time of the analysis interval. The average  $Q$  value in subregion B, which extensively contains the North Anatolian fault zone, shows relatively lower value than that in subregion A, as shown in **Fig. 8**. Average coda- $Q$  values

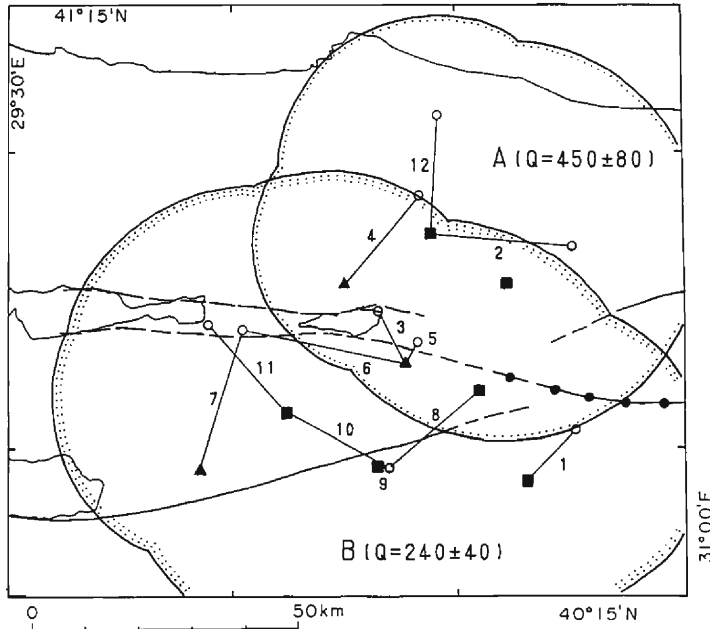


Fig. 8. Summarized coda- $Q$  distribution in the westernmost part of the North Anatolian Fault Zone. Solid and broken lines represent surface traces of active faults. The solid line with small solid circles shows the surface rupture associated with the 1967 Mudurnu earthquake<sup>10)</sup>. Coda- $Q$  values have been estimated for twelve event-station pairs (Nos. 1–12). Open circles, solid squares and solid triangles represent the location of events used for analysis, radio-linked stations and independent (OM-type) stations, respectively. From coda- $Q$  values obtained at 10 Hz, this region is divided into two subregions A and B, each of which is encircled by a composite circular arc. Averaged  $Q$  value in each subregion is indicated in parentheses with its standard deviation.

obtained at 5 Hz are 220 and 140 in subregions A and B, respectively. Similar attenuation properties can be seen also at 5 Hz.

**Fig. 9** represents the example of waveforms observed in subregions A and B. The analysis interval was about 18 seconds in common to the two events. During this interval, the coda amplitude of the event in subregion B really decays more quickly than that in subregion A, as shown in **Fig. 9(a)**. As previously described, the coda- $Q$  analysis is usually done for the lapse time greater than twice the travel time of S-waves. This lapse time is indicated by solid arrows in **Fig. 9**. If coda waves only after this time are analyzed, the result changes little, as shown in **Fig. 9(b)**. The event in subregion B has almost constant coda amplitude after the analysis interval, contrary to the other one shown with a broken straight line, as represented in **Fig. 9(b)**. This kind of feature appears when the signal-to-noise ratio is poor.

**Fig. 10** shows the frequency dependence of  $Q$  values averaged in respective subregions. According to extensive studies on coda- $Q$ <sup>13)</sup>, the  $Q$  values tend to in-

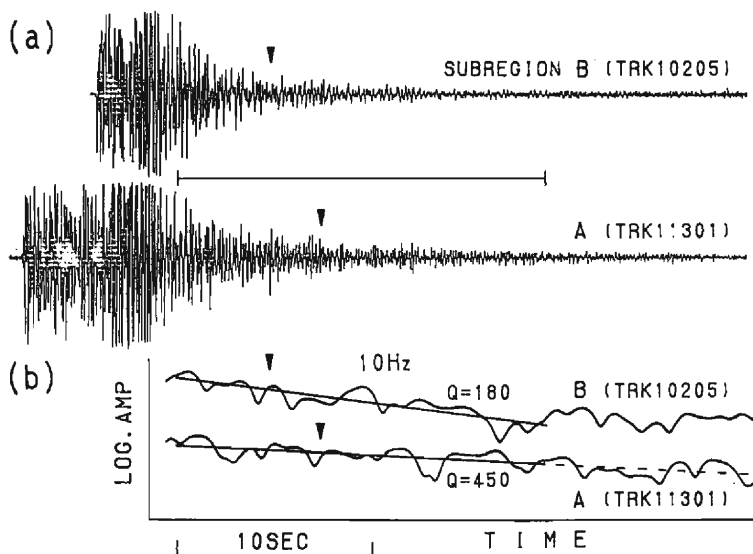


Fig. 9. (a) Example of waveforms observed in subregions A and B, which correspond to the data No. 2 and 1 in Table 1, respectively. Time axes of two events are arranged so as to take the common analysis interval, which is shown by a horizontal bar. Solid arrows indicate the time, corresponding to twice the S-wave travel time measured from the event origin time. (b) Logarithmic coda amplitude (10 Hz), in which the geometrical spreading effect is corrected, calculated from the waveforms shown in (a). The time axis is common with (a). Linear decay of amplitude is shown by the straight lines with obtained  $Q$  values.

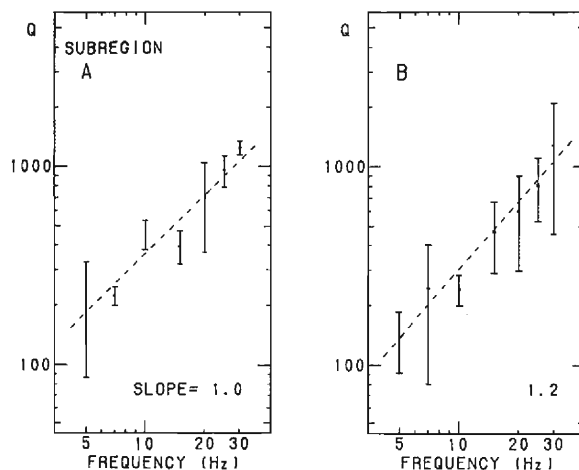


Fig. 10. Coda- $Q$  values as a function of frequency, from 5 to 30 Hz, estimated for subregions A and B. Average  $Q$  values and the standard deviation are plotted, calculated from the results of three and nine event-station pairs, respectively. Linear relationships between the logarithms of  $Q$  value and of frequency are shown by broken straight lines with the slope.

crease with frequency  $f$  in proportion to  $f^n$ , where  $n$  takes a value between about 0.5 and 1.0. This relationship was applied to our result between 5 and 30 Hz as indicated by broken straight lines with the slope  $n$  in **Fig. 10**.

#### 4. Discussion

As described in the introductory section and shown in **Fig. 2**, the western part of the North Anatolian fault zone is under tensile tectonic stress in an almost north-south direction, in contrast to the central and eastern part of the fault zone, where right-lateral strike-slip faulting is dominant. Therefore, it is important to elucidate the mode of earthquake faulting in the seismic gap region shown in **Fig. 1**.

As stated in Sec. 2.3, the focal mechanism for microearthquakes along the Izmit-Sapanca fault zone seems to be somewhat complicated, compared with that along the Iznik-Mekece fault, where the strike-slip solution agrees well with the geomorphological mode of deformation along the fault. We will discuss the focal mechanism along the Izmit-Sapanca fault zone in detail.

McKenzie<sup>15)</sup> showed that the largest aftershock ( $M5.6$ ) following the 1967 Mudurnu earthquake, which was located at about 15 km east of Sapanca Lake, had an almost pure normal-faulting mechanism with T-axes in almost the NE-SW direction as shown in **Fig. 2**. The composite focal mechanism for the present microearthquakes in the same area has been estimated to be a similar solution as shown in **Fig. 6** (region (c)). The tectonic stress field east of Sapanca Lake seems to have been constant since 1967.

Evans *et al.*<sup>15)</sup> investigated the fault plane solutions for many microearthquakes near Izmit Bay, and showed that normal faulting with some strike-slip component was dominant there. The T-axes were in the NE-SW or NNE-SSW directions. The inferred slip vectors were in about N50°E direction and the fault plane normals had some diverse directions.

Our present study has first determined the focal mechanism near Sapanca Lake as shown in **Fig. 6** (region (b)). The strike-slip solution implies that normal faulting is not dominant all along the Izmit Sapanca fault zone. The results stated above are schematically summarized in **Fig. 11**. For the region near Izmit Bay, one of typical fault strikes is represented by a broken line with arrows indicating the extent of the T-axes. The strike-slip fault near Sapanca Lake, which is inferred from the focal mechanism shown in **Fig. 6**, forms a right-stepping echelon with the Mudurnu earthquake fault (1967). The normal-faulting mechanism observed in the east of Sapanca Lake is considered to be strongly influenced by the increase of tensile stress caused by a right-lateral strike-slip movement along these two faults in echelon. The normal-faulting component observed near Izmit Bay, however, cannot be explained by this kind of interaction between the neighboring faults. It may be due to the tensile tectonic stress acting over the westernmost part of Turkey.

From the results described above, we can estimate the faulting type of a future

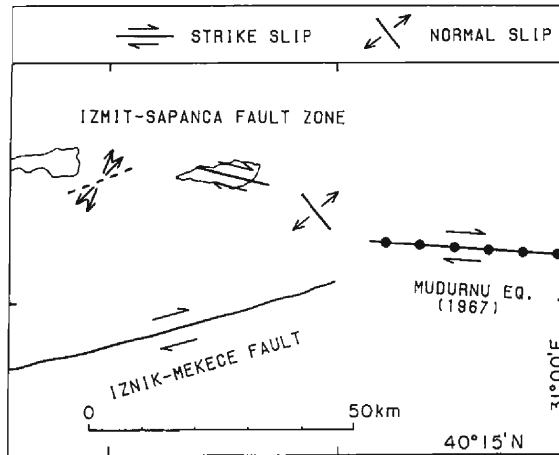


Fig. 11. Schematic illustration showing the focal mechanism in the studied area. Solid and broken lines represent the fault strike. Pairs of arrows indicate the direction of dislocation for the strike-slip fault, and the direction of T-axes for the normal-slip fault. The fault strike of the 1967 Mudurnu earthquake is from its focal mechanism<sup>15)</sup>. For the region near Izmit Bay, the fault strike (right-lateral slip) of one of typical focal mechanisms is shown by the broken line with arrows indicating the extent of T-axes<sup>6)</sup>. The normal fault in the east of Sapanca Lake is from the focal mechanism of the largest aftershock following the 1967 Mudurnu earthquake and from that of our result shown in Fig. 6. The strike-slip faults near Sapanca Lake and along the Iznik-Mekece fault are from our result.

large earthquake in the seismic gap region as follows: If it occurs along the Iznik-Mekece fault, it will have the strike-slip mechanism; but if it occurs along the Izmit-Sapanca fault zone, its faulting type may have two possibilities, strike-slip or normal-slip.

Ikeda *et al.*<sup>11)</sup> proposed a model of the tectonic movement along the Izmit-Sapanca and Iznik-Mekece fault zones, in order to explain the compressional surface deformation in the late Quaternary time along the Izmit-Sapanca fault zone. According to this model, reverse-faulting events with P-axes in about the NW-SE direction may be expected along the Izmit-Sapanca fault zone at focal depths shallower than about 6 km. Earthquakes with a flat-laying fault plane and with a slip vector in the NE or ENE direction may also be observed at focal depths of about 6 km between the Izmit-Sapanca and Iznik-Mekece fault zones. Further studies on the focal mechanism will be necessary.

Tsukuda *et al.*<sup>22)</sup> obtained low coda- $Q$  values, 75 at 5 Hz, inside the subregion B in our present study, compared with the values, 156 and 245, estimated in the surrounding region. This property is consistent with our result. These  $Q$  values, however, cannot be directly compared with our result, because they assumed  $b=1.0$  in equations (1) and (2).

Coda- $Q$  values from local earthquakes have been extensively studied in various regions. According to Aki<sup>2)</sup> and Jin *et al.*<sup>13)</sup>, the coda- $Q$  value tends to be lower

and the value  $n$ , which was explained in the previous section, also tends to be larger in active tectonic regions. The value  $n$  in subregion B is larger than that in subregion A as shown in **Fig. 10**. This agrees with the general tendency described above.

Singh and Herrmann<sup>18)</sup> studied a spatial distribution of coda- $Q$  values over the continental United States, and found a negative correlation between  $Q$  values and the seismic activity. The crust in active regions is supposed to have a strong inhomogeneity, seen from the dense distribution of active faults and high seismicity. This inhomogeneity is considered to be the main factor of the above stated attenuation property of seismic waves. In our result shown in **Fig. 8**, the spatial distribution of coda- $Q$  values is also considered to suggest the inhomogeneous structures of the crust due to the earthquake faulting along the North Anatolian fault zone.

Temporal change of coda- $Q$  values preceding large or medium scale earthquakes has been reported<sup>14,21)</sup>. Coda- $Q$  values may be one of important parameters indicating the stress state in the crust, from a viewpoint of the earthquake prediction. Further observations and studies on microseismic activity, focal mechanism, coda- $Q$ , etc. are to be continued in this seismic gap region.

## 5. Concluding Remarks

We carried out a short-term observation of microearthquakes in the seismic gap region in the western part of the North Anatolian fault zone. The results of our analyses are as follows:

1. Microseismic activity is rather high along the Izmit-Sapanca fault zone. On the other hand, the activity is low along the Iznik-Mekece fault. This feature seems to have continued over the past several years, in view of previous research.
2. The fault plane solution of strike-slip type was obtained for a microearthquake along the Iznik-Mekece fault. This solution coincides well with the geomorphological observations of right-lateral strike-slip movement along this fault. On the other hand, the solutions of both strike-slip and normal-faulting types were determined for microearthquakes along the Izmit-Sapanca fault zone.
3. Relatively lower coda- $Q$  values were estimated, at frequencies of 5 and 10 Hz, around the Izmit-Sapaca and Iznik-Mekece fault zones, in comparison with the region north of the fault zones.

## Acknowledgements

The authors are grateful to Prof. M. Dizer, Director of Kandilli Observatory and Earthquake Research Institute, Boğaziçi University, Turkey, for his support to our work. The authors wish also to thank Dr. Naoto Oshiman of Nihon University and Prof. Jun'ichiro Miyakoshi of Tottori University for their help to our work. Thanks are extended to Mr. Şerif Bariş, Ms. Oya Yazici and Mr. Nafiz Kafadar

at Kandilli Observatory for assisting us in the observation. The authors are also grateful to Prof. H. Berckhemer of University of Frankfurt, G.F.R., for kindly offering us the seismic data of Turkish-German Earthquake Prediction Research. Comments by anonymous reviewers were very helpful in improving the manuscript. This study was supported by a Grant-in-Aid for International Scientific Research, No. 63041054, Ministry of Education, Science and Culture, Japan.

### References

- 1) Aki, K.: Scattering and attenuation of shear waves in the lithosphere, *J. Geophys. Res.*, Vol. 85, 1980, pp. 6496–6504.
- 2) Aki, K.: Scattering and attenuation of high-frequency body waves (1–25 Hz) in the lithosphere, *Phys. Earth Planet. Inter.*, Vol. 26, 1981, pp. 241–243.
- 3) Aki, K. and B. Chouet: Origin of coda waves: Source, attenuation and scattering effects, *J. Geophys. Res.*, Vol. 80, 1975, pp. 3322–3342.
- 4) Ambraseys, N. N.: Some characteristic features of the Anatolian fault zone, *Tectonophysics*, Vol. 9, 1970, pp. 143–165.
- 5) Crampin, S., R. Evans and S. B. Üçer: Analysis of local earthquakes: the Turkish Dilatancy Projects (TDP1 and TDP2), *Geophys. J. R. Astr. Soc.*, Vol. 83, 1985, pp. 1–16.
- 6) Evans, R., I. Asudeh, S. Crampin and S. B. Üçer: Tectonics of the Marmara Sea region of Turkey: new evidence from micro-earthquake fault plane solutions, *Geophys. J. R. Astr. Soc.*, Vol. 83, 1985, pp. 47–60.
- 7) Honkura, Y. and A. M. Işikara: Multidisciplinary research on fault activity in the western part of the North Anatolian Fault Zone, 1988, pp. 1–120.
- 8) Honkura, Y. and A. M. Işikara: Multidisciplinary research on fault activity in the western part of the North Anatolian Fault Zone (2), 1989, pp. 1–162.
- 9) Iio, Y., C. Gürbüz, K. Nishigami, A. Pinar, N. Aybey, S. B. Üçer, Y. Honkura and A. M. Işikara: Microseismic activity around the western extension of the 1967 Mudurnu earthquake fault, *Tectonophysics*, (in press).
- 10) Ikeda, Y.: Geomorphological observations of the North Anatolian Fault Zone, west of Mudurnu, in *Multidisciplinary Research on Fault Activity in the Western Part of the North Anatolian Fault Zone*, (Eds., Y. Honkura and A. M. Işikara), 1988, pp. 6–14.
- 11) Ikeda, Y., Y. Honkura and A. M. Işikara: Quaternary compressional deformation in the Izmit-Sapaca trough, western Turkey, and its implications for the present tectonics near the western termination of the North Anatolian fault zone, in *Multidisciplinary Research on Fault Activity in the Western Part of the North Anatolian Fault Zone (2)*, (Eds., Y. Honkura and A. M. Işikara), 1989, pp. 45–56.
- 12) Jackson, J. and D. McKenzie: Active tectonics of the Alpine-Himalayan Belt between western Turkey and Pakistan, *Geophys. J. R. Astr. Soc.*, Vol. 77, 1984, pp. 185–264.
- 13) Jin, A., T. Cao and K. Aki: Regional change of coda  $Q$  in the oceanic lithosphere, *J. Geophys. Res.*, Vol. 90, 1985, pp. 8651–8659.
- 14) Jin, A. and K. Aki: Temporal change in coda  $Q$  before the Tangshan earthquake of 1976 and the Haicheng earthquake of 1975, *J. Geophys. Res.*, Vol. 91, 1986, pp. 665–673.
- 15) McKenzie, D.: Active tectonics of the Mediterranean region, *Geophys. J. R. Astr. Soc.*, Vol. 30, 1972, pp. 109–185.
- 16) McKenzie, D.: Active tectonics of the Alpine-Himalayan belt: the Aegean Sea and surrounding regions, *Geophys. J. R. Astr. Soc.*, Vol. 55, 1978, pp. 217–254.
- 17) Oike, K. and K. Matsumura: A new recording system of seismic waves using audio recorder, *Zisin (J. Seismol. Soc. Jpn.)*, Ser. 2, Vol. 38, 1985, pp. 359–364 (in Japanese).
- 18) Singh, S. and R. B. Herrmann: Regionalization of crustal coda  $Q$  in the continental United States, *J. Geophys. Res.*, Vol. 88, 1983, pp. 527–538.
- 19) Sipahioğlu, S. and T. Matsuda: Geology and quaternary fault in the Iznik-Mekece area, in



- Electric and Magnetic Research on Active Faults in the North Anatolian Fault Zone, (Eds., A. M. İşikara and Y. Honkura), 1986, pp. 25-41.
- 20) Toksöz, M. N., A. F. Shakal and A. J. Michael: Space-time migration of earthquakes along the North Anatolian fault zone and seismic gaps, *Pure Appl. Geophys.*, Vol. 117, 1979, pp. 1258-1270.
  - 21) Tsukuda, T.: Coda-Q before and after the 1983 Misasa earthquake of M 6.2, Tottori Prefecture, Japan, *Pure Appl. Geophys.*, Vol. 128, 1988, pp. 261-279.
  - 22) Tsukuda, T., K. Satake, Y. Honkura, S. B. Üçer and A. M. İşikara: Low seismicity, low coda-Q and discontinuities of the upper crust in the vicinity of the Iznik-Mekece Fault, the North Anatolian Fault Zone, Turkey, *Bull. Earthq. Res. Inst.*, Vol. 63, 1988, pp. 327-348.
  - 23) Üçer, S. B., S. Crampin, R. Evans, A. Miller and N. Kafadar: The MARNET radiolinked seismometer network spanning the Marmara Sea and the seismicity of Western Turkey, *Geophys. J. R. astr. Soc.*, Vol. 83, 1985, pp. 17-30.
  - 24) Watanabe, H.: Determination of earthquake magnitude at regional distance in and near Japan, *Zisin (J. Seismol. Soc. Jpn.)*, Ser. 2, Vol. 24, 1971, pp. 189-200 (in Japanese).
  - 25) Weigelt, E., H. Berckhemer, B. Baier, R. Ates, A. Yatman and O. Ozel: Seismic observations in the Mudurnu Valley Test Area at the North Anatolian Fault Zone, in *Turkish-German Earthquake Research Project*, (Eds., J. Zschau and O. Ergunay), 1998, pp. 45-56.